



High-precision Q -value measurement and nuclear matrix element calculations for the double- β decay of ^{98}Mo

D. A. Nesterenko^{1,a}, L. Jokiniemi², J. Kotila^{1,3}, A. Kankainen¹, Z. Ge¹, T. Eronen¹, S. Rinta-Antila¹, J. Suhonen¹

¹ Accelerator Laboratory, Department of Physics, University of Jyväskylä, P.O. Box 35, FI-40014 Jyväskylä, Finland

² Department of Quantum Physics and Astrophysics and Institute of Cosmos Sciences, University of Barcelona, 08028 Barcelona, Spain

³ Sloane Physics Laboratory, Center for Theoretical Physics, Yale University, New Haven, CT 06520-8120, USA

Received: 9 November 2021 / Accepted: 22 February 2022 / Published online: 14 March 2022

© The Author(s) 2022

Communicated by Klaus Blaum

Abstract The ^{98}Mo double-beta decay Q -value has been measured, and the corresponding nuclear matrix elements of neutrinoless double-beta ($0\nu\beta\beta$) decay and the standard two-neutrino double-beta ($2\nu\beta\beta$) decay have been provided by nuclear theory. The double-beta decay Q -value has been determined as $Q_{\beta\beta} = 113.668(68)$ keV using the JYFLTRAP Penning trap mass spectrometer. It is in agreement with the literature value, $Q_{\beta\beta} = 109(6)$ keV, but almost 90 times more precise. Based on the measured Q -value, precise phase-space factors for $2\nu\beta\beta$ decay and $0\nu\beta\beta$ decay, needed in the half-life predictions, have been calculated. Furthermore, the involved nuclear matrix elements have been computed in the proton–neutron quasiparticle random-phase approximation (pnQRPA) and the microscopic interacting boson model (IBM-2) frameworks. Finally, predictions for the $2\nu\beta\beta$ decay are given, suggesting a much longer half-life than for the currently observed cases.

1 Introduction

Double-beta ($\beta\beta$) decay is a nuclear process in which two neutrons turn into protons (or vice versa) and two electrons are emitted. In the standard, two-neutrino double-beta ($2\nu\beta\beta$) decay, the emitted electrons are accompanied by two antineutrinos and hence the lepton number is conserved. Such process has already been observed in about a dozen nuclei, where β decay is energetically forbidden or very suppressed [1]. However, there is also a hypothetical version of $\beta\beta$ decay, namely neutrinoless double-beta ($0\nu\beta\beta$) decay, where only two electrons are emitted. This process violates the lepton-number conservation law of the standard model (SM) of

particle physics by two units, since two leptons are created. The process is only possible if neutrino is a Majorana particle (meaning its own antiparticle) first hypothesized by Ettore Majorana in 1937 [2]. The observation of $0\nu\beta\beta$ decay could therefore answer the open questions about beyond-SM physics such as the matter-antimatter symmetry of the Universe [3,4] and the nature of neutrinos [5–9]. The decay rates of both decay modes are strong functions of the Q -value. $0\nu\beta\beta$ -decay scales with the fifth power of the Q -value and $2\nu\beta\beta$ -decay with the eleventh power.

The neutrinoless mode is under intense searches by several large-scale experiments worldwide [10–16], with the most stringent half-life limits given by $t_{1/2}^{0\nu} \gtrsim 10^{26}$ years, while the measured half-lives of $2\nu\beta\beta$ decay are in the order of $t_{1/2}^{2\nu} \sim 10^{18} - 10^{24}$ years [1]. Another intriguing aspect of $0\nu\beta\beta$ decay is that the half-life of the process is inversely proportional to the square of the effective Majorana mass, which depends on the neutrino masses. Hence, one could obtain estimates for the neutrino masses (at present, only the differences of the squares are known) from the measured half-lives [17, 18]. The next-generation $\beta\beta$ -decay experiments are aiming at fully covering the inverted-hierarchy (meaning that the neutrino mass states follow the ordering $m_3 < m_1 \lesssim m_2$) region of the neutrino masses [19]. However, in order to interpret the results, one needs reliable phase-space factors and $\beta\beta$ -decay nuclear matrix elements (NMEs), which need to be provided by nuclear theory. While the phase-space factors can be accurately calculated [20], the present predictions for the $0\nu\beta\beta$ -decay NMEs from different theory frameworks disagree by more than a factor of two [7].

In the present paper, we study one of the possible $\beta\beta$ emitters, ^{98}Mo . So far, there has been no direct Q -value measurement for the double-beta decay transition between the nuclear ground states $^{98}\text{Mo} \rightarrow ^{98}\text{Ru}$. The literature Q -value,

^a e-mail: dmitrii.nesterenko@jyu.fi (corresponding author)

109(6) keV [21], has been limited by the uncertainty in the mass value of ^{98}Ru . It is mainly based on the mass difference between C_7H_{14} and ^{98}Ru measured using a sixteen-inch double-focusing mass spectrometer in 1960s [22]. In this work, we determine the Q value by a direct frequency-ratio measurement of singly-charged $^{98}\text{Mo}^+$ and $^{98}\text{Ru}^+$ ions in the JYFLTRAP Penning trap [23]. In addition, we have measured the Q -value for the double-electron capture of ^{96}Ru and compared it to the high-precision measurement ($\delta m/m \approx 1.4 \times 10^{-9}$) done using the SHIPTRAP Penning trap [24].

Based on the measured Q -value for the $\beta\beta$ -decay of ^{98}Mo , we calculate the phase-space factors for the two-neutrino and the neutrinoless decay modes. Furthermore, we calculate the NMEs for the two decay modes in two different theory frameworks that are well established for calculating the NMEs in medium-heavy to heavy nuclei: proton-neutron quasiparticle random-phase approximation (pnQRPA) [25, 26] and microscopic interacting boson model (IBM-2) [27, 28]. This is the first time the ^{98}Mo double-beta decay matrix elements are calculated in no-core pnQRPA and IBM-2 frameworks. Due to the low Q -value, the $2\nu\beta\beta$ -decay has not been measured – hence, we give estimates for both the $2\nu\beta\beta$ -decay and $0\nu\beta\beta$ -decay half-lives based on the calculated NMEs and phase-space factors.

2 Experimental method and results

The Q -value measurements have been performed using the JYFLTRAP Penning trap mass spectrometer [23] at the Ion Guide Isotope Separator On-Line (IGISOL) facility [29]. The ions of interest were separately produced using two electric discharge ion sources, one with natural ruthenium in the IGISOL target chamber [30] and the other with natural molybdenum at the offline ion source station [31]. Most of the ions were produced as singly-charged and accelerated to 30 keV. An electrostatic deflector selected ions from one ion source at a time, blocking the ions from the other source. The ions were mass-separated using a 55° dipole magnet and the continuous beam with the selected mass number A was injected into a gas-filled radiofrequency quadrupole (RFQ) [32]. The cooled and bunched ion beam after the RFQ was transported to the JYFLTRAP Penning traps placed inside a 7-T superconducting magnet.

In the first (preparation) trap the ions were cooled, centered and additionally purified using a mass-selective buffer gas cooling technique [33]. In the second (measurement) trap the cyclotron frequency for an ion with mass m and charge q in the magnetic field B , given by

$$\nu_c = \frac{1}{2\pi} \frac{q}{m} B, \quad (1)$$

was measured employing the phase-imaging ion-cyclotron-resonance (PI-ICR) technique [34–36].

The ion's cyclotron frequency ν_c was determined as a sum of its radial-motion frequencies in the trap, a magnetron frequency ν_- and a modified cyclotron frequency ν_+ . The measurements followed the scheme described in Ref. [35]. Two excitation patterns were applied alternately in order to determine the accumulated magnetron and cyclotron phases of the ion motion. After injecting the ions into the measurement trap, the coherent component of the magnetron motion was reduced by applying 600- μs dipolar radiofrequency (rf) pulse at the magnetron frequency ν_- . Then, the cyclotron motion of the ions was excited to an amplitude of about 1 mm through application of a 100- μs dipolar rf pulse at the modified cyclotron frequency ν_+ . After the excitation, the ion's cyclotron motion was converted into the magnetron motion via a 2-ms quadrupolar rf pulse at the frequency close to the cyclotron frequency ν_c . The ions accumulated the magnetron-motion phase during the phase accumulation time t_{acc} of free rotation and were then extracted from the trap. For the measurement of the cyclotron-motion phase the ions accumulated the cyclotron phase after ν_+ -pulse for the phase accumulation time t_{acc} , which was followed by a conversion pulse applied before the extraction from the trap. The radial motion phase of the ions extracted from the trap was projected onto a position-sensitive detector (microchannel plate detector with a delay line anode).

The positions of the magnetron and cyclotron phase images on the detector, defined by the polar angles α_- and α_+ , correspondingly, with respect to the trap center, were chosen such that the angle $\alpha_c = \alpha_+ - \alpha_-$ did not exceed a few degrees. It is required to minimize the systematic shifts due to the distortion of the projection on the detector and reduce the influence from the conversion of the cyclotron motion to the magnetron motion [35]. The cyclotron frequency is determined from the angle between two phase images as:

$$\nu_c = \nu_- + \nu_+ = \frac{\alpha_c + 2\pi n}{2\pi t_{acc}}, \quad (2)$$

where n is the full number of revolutions, which the studied ions would perform in a magnetic field B in absence of electric field during a phase accumulation time t_{acc} .

The phase spots and the center spot were alternately accumulated during a single 4.5-min cyclotron frequency measurement (see Fig. 1). About 300 ions were collected for each spot. Any residual magnetron and cyclotron motion could lead to shifts of the phase position. To eliminate these effects, the start time of the cyclotron excitation was repeatedly scanned over a magnetron period ($\approx 600 \mu\text{s}$) and the start time of the extraction pulse was scanned over a cyclotron period ($\approx 0.9 \mu\text{s}$).

The cyclotron frequencies of the parent nuclide ν_c^p and the daughter nuclide ν_c^d were alternately measured changing

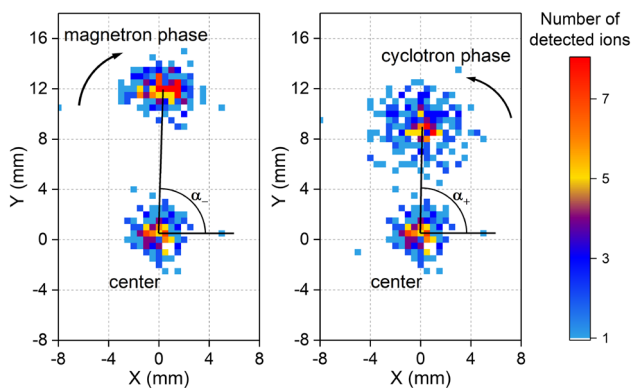


Fig. 1 Projection of the trap center and accumulated phase spots for $^{98}\text{Mo}^+$ ions on the position-sensitive MCP detector in a single 4.5-min cyclotron frequency measurement with the PI-ICR method. The phase accumulation time t_{acc} was about of 500 ms

every 4.5 minutes. The frequency ν_c^d measured before and after the ν_c^p measurement, was linearly interpolated to the time of the ν_c^p measurement and a single cyclotron frequency ratio $R_i = \nu_c^d / \nu_c^p$ was determined. The systematic uncertainty due to non-linear changes of the magnetic field was negligible compared to the achieved statistical uncertainty [37]. The final cyclotron frequency ratio \bar{R} was calculated as a weighted mean of R_i . The ions of the parent and daughter nuclides were measured in similar conditions to minimize a possible systematic shift of the frequency ratio due to imperfections of the measurement trap. Mass-dependent systematic effects are negligible compared to the statistical

uncertainty for mass doublets [38]. Count-rate class analysis [38, 39] was performed and no correlations between the frequency ratios and the number of detected ions per bunch were observed. Up to 5 ions/bunch were taken into account in the analysis.

The Q -value is calculated from the cyclotron frequency ratio as

$$Q = (M_p - M_d) c^2 = \left(\frac{\nu_c^d}{\nu_c^p} - 1 \right) (M_d - m_e) c^2, \quad (3)$$

where M_p and M_d are the atomic masses and ν_c^p and ν_c^d the cyclotron frequencies of the parent and daughter nuclides, correspondingly, m_e is the electron mass and c is the speed of light in vacuum. The difference in binding energies of valence electron in Mo and Ru is less than 1 eV [40], and has been neglected. The atomic mass unit used in the analysis is $u = 931494.10242(28) \text{ keV}/c^2$ [41].

The cyclotron frequency ratios $R_i = \nu_c(^{98}\text{Ru}^+) / \nu_c(^{98}\text{Mo}^+)$, measured at JYFLTRAP, are shown in Fig. 2. The phase accumulation time t_{acc} of about 500 ms was chosen to ensure that the cyclotron spot was not overlapping with any possible isobaric contamination on the detector. The final weighted mean frequency ratio is $\bar{R} = 1.00000124639(74)$ resulting in a $Q_{\beta\beta}$ -value of 113.668(68) keV. Using the determined $Q_{\beta\beta}$ -value of ^{98}Mo and the mass-excess value of ^{98}Mo from AME20, $-88115.98(17) \text{ keV}$ [21], we also improve the mass-excess value for ^{98}Ru considerably, from $-88225(6) \text{ keV}$ in AME20 [21] to $-88229.65(19) \text{ keV}$.

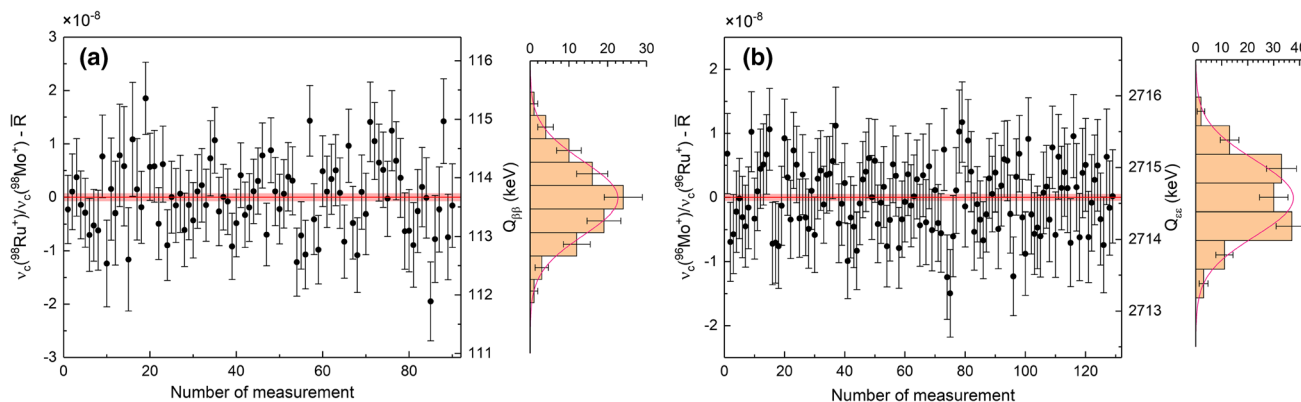


Fig. 2 Cyclotron frequency ratios **a** $\bar{R} = \nu_c(^{98}\text{Ru}^+) / \nu_c(^{98}\text{Mo}^+)$ and **b** $\bar{R} = \nu_c(^{96}\text{Mo}^+) / \nu_c(^{96}\text{Ru}^+)$ measured in this work. The red band represents the total 1σ uncertainty of the weighted mean frequency ratio \bar{R} .

For \bar{R} see Table 1. Also the distribution of the individual measurements within $\pm 200 \text{ eV}$ bins is shown indicating a normal distribution

Table 1 The weighted means (\bar{R}) of the measured frequency ratios $R = \nu_c(\text{daughter}) / \nu_c(\text{parent})$ and the corresponding Q -values for the studied transitions

Transition	Frequency ratio \bar{R}	Q -value (keV)	Lit. Q -value (keV)	Difference (keV)
$^{98}\text{Mo} \rightarrow ^{98}\text{Ru}$	1.000 001 246 39 (74)	113.668 (68)	109 (6) [21]	4.7 (60)
$^{96}\text{Ru} \rightarrow ^{96}\text{Mo}$	1.000 030 386 86 (55)	2714.583 (50)	2714.51 (13) [24]	0.073 (139)

The literature Q -values and differences to the literature values are also given

Similarly, the Q -value of double-electron capture in ^{96}Ru was measured using the PI-ICR technique with the phase accumulation time t_{acc} of about 510 ms. The results are given in Table 1. The measured $Q_{e\bar{e}}$ -value of ^{96}Ru , 2714.583(50) keV, is in a good agreement with the SHIPTRAP $Q_{e\bar{e}}$ -value, 2714.51(13) keV [24], and 2.6 times more precise. This measurement provides an additional cross-check of our accuracy with Mo and Ru ions in the studied mass region.

3 Theory predictions for double-beta decay of ^{98}Mo

3.1 Two-neutrino double-beta decay

The $2\nu\beta\beta$ -decay half-life can be written in the form

$$[t_{1/2}^{2\nu}]^{-1} = G_{2\nu} \left(g_A^{\text{eff}} \right)^4 \left| M^{2\nu} \right|^2, \quad (4)$$

where $G_{2\nu}$ is a phase-space factor for the final-state leptons [20] for the two-neutrino mode and $M^{2\nu}$ is the $2\nu\beta\beta$ -decay NME. Here g_A^{eff} is the effective value of the axial-vector coupling, quenched relative to the free-nucleon value $g_A \simeq 1.27$, as found in many different nuclear-structure calculations for the medium-mass and heavy nuclei along the years (see the recent reviews [9, 42]). The NME can be written as

$$M^{2\nu} = M_{\text{GT}}^{2\nu} + \left(\frac{g_V}{g_A} \right)^2 M_{\text{F}}^{2\nu}, \quad (5)$$

with Gamow–Teller (GT) and Fermi (F) parts and the vector coupling $g_V = 1.0$ [25]. In the case of $2\nu\beta\beta$ decay, if isospin is a good quantum number, the Fermi matrix elements should identically vanish. Thus, in both pnQRPA and IBM-2 calculations the Fermi part of the matrix element is set to zero in order to restore isospin symmetry, as explained in Sect. 3.4.

3.2 Neutrinoless double-beta decay

The $0\nu\beta\beta$ -decay half-life can be written as [7]

$$[t_{1/2}^{0\nu}]^{-1} = G_{0\nu} \left(g_A^{\text{eff}} \right)^4 \left| M^{0\nu} \right|^2 \frac{m_{\beta\beta}^2}{m_e^2}, \quad (6)$$

where $G_{0\nu}$ is a phase-space factor for the final-state leptons [20] in the neutrinoless mode, and $M^{0\nu}$ is the light-neutrino-exchange $0\nu\beta\beta$ -decay NME. The effective mass $m_{\beta\beta} = \sum_i U_{ei} m_i$ characterizes the lepton-number violation and depends on the neutrino masses m_i and mixing matrix U .

The matrix element $M^{0\nu}$ in Eq. (6) consists of Gamow–Teller (GT), Fermi (F) and tensor (T) parts and can be written as [7]

$$M^{0\nu} = M_{\text{GT}}^{0\nu} - \left(\frac{g_V}{g_A} \right)^2 M_{\text{F}}^{0\nu} + M_{\text{T}}^{0\nu}. \quad (7)$$

3.3 Phase-space factors

The key ingredient for the evaluation of phase-space factors (PSF) in single- and double- β decay are the electron wave functions. These energy-dependent wave functions are used to form decay-mechanism specific combinations and then integrated over available electron energies up to the endpoint energy dictated by the Q -value. A general theory of phase-space factors in $\beta\beta$ -decay was developed years ago by Doi et al. [43, 44] following the previous work of Primakoff and Rosen [45]. It was reformulated by Tomoda [46] who also presented results for selected nuclei. However, in these earlier calculations approximate expression for the electron wave functions at the nucleus was used. Here we evaluate the PSFs using exact Dirac electron wave functions and including screening by the electron cloud by following the procedure given in Ref. [20]. The obtained PSFs for ^{98}Mo are: $G_{0\nu} = 6.18 \times 10^{-18} \text{year}^{-1}$ and $G_{2\nu} = 3.71 \times 10^{-29} \text{year}^{-1}$ for the neutrinoless and two-neutrino double-beta decay, respectively. These PSFs can then be combined with nuclear matrix elements that are dimensionless. Even though the newly measured Q -value is slightly larger than the one used in previous calculations of Boehm and Vogel [47], and Doi et al. [48], the obtained phase-space factors are slightly smaller due the use of exact Dirac electron wave functions, as was also reported in Ref. [20] for several other $\beta\beta$ -decay candidates.

3.4 Nuclear matrix elements

The pnQRPA calculations in the present study are based on the spherical version of pnQRPA with large no-core single-particle bases, similarly as in Refs. [49, 50]. The single-particle bases consist of 25 orbitals - from the lowest $0s_{1/2}$ orbit up to the $0i_{13/2}$ orbit. We take the single-particle energies from a Coulomb-corrected Woods-Saxon potential [51]. The quasiparticle spectra, needed in the pnQRPA diagonalization, are obtained by solving the BCS equations using a pairing interaction based on the Bonn-A meson-exchange potential [52] for protons and neutrons separately. The interaction is fine-tuned by adjusting the pairing parameters to reproduce the phenomenological pairing gaps. The residual Hamiltonian of the pnQRPA calculation contains two adjustable parameters: the particle-particle g_{pp} and the particle-hole g_{ph} parameters [53]. The particle-hole parameter is adjusted to reproduce the location of the Gamow–Teller giant resonance in ^{98}Tc . It is a well-known feature [53] that the β - and $\beta\beta$ -decay NMEs are sensitive to the value of particle-particle parameter g_{pp} , as demonstrated in the present calculations in Fig. 3. Here we follow the so-called partial isospin restoration scheme [54], and divide the parameter into isoscalar ($T = 0$) and isovector ($T = 1$) parts which multiply the isoscalar and isovector channels of the

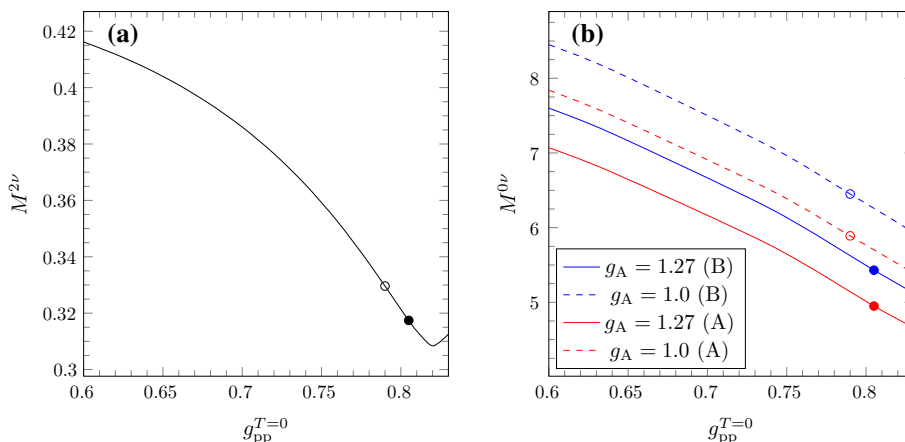


Fig. 3 **a** $2\nu\beta\beta$ -decay and **b** $0\nu\beta\beta$ -decay NMEs of the transition $^{98}\text{Mo}(0_{\text{g.s.}}^+) \rightarrow ^{98}\text{Ru}(0_{\text{g.s.}}^+)$ as functions of the particle-particle parameter $g_{pp}^{T=0}$ in the pnQRPA framework. The solid (open) circles cor-

respond to the $g_{pp}^{T=0}$ adjusted to the log ft -value of the transition $^{98}\text{Nb}(1_{\text{g.s.}}^+) \rightarrow ^{98}\text{Mo}(0_{\text{g.s.}}^+)$ with $g_A^{\text{eff}} = 1.27$ ($g_A^{\text{eff}} = 1.0$). 'A' refers to the Argonne and 'B' to the CD-Bonn SRC-parametrization

calculations, respectively. The strength $g_{pp}^{T=1}$ of the isovector channel is then adjusted so that the Fermi part of the $2\nu\beta\beta$ -decay NME vanishes. Ideally, the isoscalar strength $g_{pp}^{T=0}$ would then be fixed so that $M_{\text{GT}}^{2\nu}$ reproduces the measured $2\nu\beta\beta$ -decay half-life, but since it has not been measured for ^{98}Mo , we adjust $g_{pp}^{T=0}$ to the observed Gamow-Teller transition $^{98}\text{Nb}(1_{\text{g.s.}}^+) \rightarrow ^{98}\text{Mo}(0_{\text{g.s.}}^+)$ with $\log ft = 4.72$, instead.

The wave functions and excitation energies of the states in an odd-odd nucleus, needed in $\beta\beta$ -decay calculations, are then obtained from a pnQRPA diagonalization based on a neighboring even-even reference nucleus [55]. Here, due to the involved two steps of the $\beta\beta$ decay, they are computed in the intermediate odd-odd nucleus ^{98}Tc by starting from the ^{98}Mo and ^{98}Ru reference nuclei. Since the Fermi part of the $2\nu\beta\beta$ NMEs is forced to zero, the $2\nu\beta\beta$ decay runs only through the 1^+ virtual states of the intermediate nucleus. Hence, the $2\nu\beta\beta$ -decay NME is calculated by summing over the 1^+ states. The Gamow-Teller part is computed as

$$M_{\text{GT}}^{2\nu} = \sum_{m,n} \left(0_{\text{gs},f}^+ \left\| \sum_k t_k^- \sigma_k \right\| 1_m^+ \right) \langle 1_m^+ | 1_n^+ \rangle \times \left(1_n^+ \left\| \sum_k t_k^- \sigma_k \right\| 0_{\text{gs},i}^+ \right) / (D_m / m_e c^2), \quad (8)$$

D_m being the energy denominator $D_m = (Q_{\beta\beta} + 2m_e c^2) / 2 + E(1_m^+) - E_p$, where E_p is the energy of the ground state in the parent nucleus and $E(1_m^+)$ is the average of the excitation energies of the m th 1^+ state in a pnQRPA calculations based on the initial and final nuclei ground-states. σ_k is the Pauli spin matrix and t_k^- is the isospin operator. The factor $\langle 1_m^+ | 1_n^+ \rangle$ is the overlap between the two sets of 1^+ states [25, 49].

On the other hand, $0\nu\beta\beta$ decays run through all J_i^π states in the intermediate nucleus. In the pnQRPA framework,

the $0\nu\beta\beta$ -decay NMEs $M_K^{0\nu}$, $K = \text{F, GT, T}$ are calculated without resorting to the so-called closure approximation by explicitly summing over the intermediate states as

$$M_K^{0\nu} = \sum_{J^\pi, k_1, k_2, \mathcal{J}} \sum_{p, p', n, n'} (-1)^{j_n + j_{p'} + J + \mathcal{J}} \sqrt{2\mathcal{J} + 1} \times \left\{ \begin{matrix} j_p & j_n & J \\ j_{n'} & j_{p'} & \mathcal{J} \end{matrix} \right\} (pp' : \mathcal{J} || \mathcal{O}_K || nn' : \mathcal{J}) \times \left(0_f^+ \left\| \left[c_{p'}^\dagger, \tilde{c}_{n'} \right]_J \right\| \left| J_{k_1}^\pi \right\rangle \langle J_{k_2}^\pi \right| \left(J_{k_2}^\pi \left\| \left[c_p^\dagger, \tilde{c}_n \right]_J \right\| \left| 0_i^+ \right\rangle \right), \quad (9)$$

where \mathcal{J} is the nucleon pair angular momentum, k_1 (k_2) labels the different pnQRPA solutions for a given J^π based on the final (initial) nucleus of the decay. The quantity inside the curly brackets is a Wigner $6j$ -symbol. The operators \mathcal{O}_K can be written in the form

$$\begin{aligned} \mathcal{O}_F &= h_F(r, E_k) [f_{\text{SRC}}(r)]^2, \\ \mathcal{O}_{\text{GT}} &= h_{\text{GT}}(r, E_k) [f_{\text{SRC}}(r)]^2 \sigma_1 \cdot \sigma_2, \\ \mathcal{O}_T &= h_T(r, E_k) [f_{\text{SRC}}(r)]^2 S_{12}^T, \end{aligned} \quad (10)$$

where h_K is the so-called neutrino potential, $r = |\mathbf{r}_1 - \mathbf{r}_2|$ is the distance between the decaying nucleons, f_{SRC} is a function taking into account the short-range correlations, and S_{12}^T is the spin tensor operator. For further details, see e.g. [25, 26].

Another frequently used model to evaluate $\beta\beta$ NMEs is the microscopic interacting boson model (IBM-2) [56, 57]. The method of evaluation is discussed in detail in Refs. [27, 28]. The logic of the method is to map [58] the fermion Hamiltonian H onto a boson space and evaluate it with bosonic wave functions. The single-particle and -hole energies and strengths of interaction were evaluated and discussed in detail in Ref. [59] where the occupancies of the single-particle levels were calculated in order to satisfy a twofold goal: to assess

Table 2 The $2\nu\beta\beta$ -decay NMEs and the resulting half-lives with different effective g_A values for the transition $^{98}\text{Mo} \rightarrow ^{98}\text{Ru}$ calculated in the pnQRPA and IBM-2 frameworks

g_A^{eff}	$M^{2\nu}$		$t_{1/2}^{2\nu} (10^{29} \text{ y})$	
	pnQRPA	IBM-2	pnQRPA	IBM-2
1.27	0.317	0.380	1.031	0.718
1.0	0.330	0.380	2.475	1.867

the goodness of the single-particle energies and to check the reliability of the used wave functions. Both tests are particularly important in the case of nuclei involved in double beta decay, as they affect the evaluation of the NMEs and thus their reliability [60].

In IBM-2 the isospin is restored by modifying the mapped operator by imposing the condition that $M_F^{2\nu} = 0$. This condition is simply implemented in the calculation by replacing the radial integrals of Appendix A of Ref. [27] with ones given in Eqs. (9) and (10) in [28] that guarantee that the Fermi matrix elements vanish for $2\nu\beta\beta$ decay, as discussed in [28]. This replacement also reduces the Fermi matrix elements for $0\nu\beta\beta$ decay by quenching the monopole term from the multipole expansion of the matrix element. Even though the method of isospin restoration is similar in spirit to that of pnQRPA, it is different in practise.

In the IBM-2 calculations closure approximation is assumed. The main idea behind the closure approximation is to replace the energies of the intermediate states with an average energy, and then the sum over the intermediate states can be removed by using the completeness relation. In IBM-2 the Gamow–Teller part for $2\nu\beta\beta$ decay can thus be written as

$$M_{\text{GT}}^{2\nu} = \left(0_{\text{gs},f}^+ \left\| \sum_{k,k'} t_k^- t_{k'}^- \sigma_k \cdot \sigma_{k'} \right\| 0_{\text{gs},i}^+ \right) / (\tilde{A}/m_e c^2), \tag{11}$$

where $\tilde{A} = (Q_{\beta\beta} + 2m_e c^2)/2 + \langle E_N \rangle - E_p$ is the so called closure energy including the suitably chosen average excitation energy $\langle E_N \rangle$ in the intermediate odd-odd nucleus. In a similar manner also the $0\nu\beta\beta$ decay calculation is simplified in closure approximation depending only on the initial and

Table 4 The $0\nu\beta\beta$ -decay half-lives with different effective g_A values for the transition $^{98}\text{Mo} \rightarrow ^{98}\text{Ru}$ calculated in the pnQRPA and IBM-2 frameworks

g_A^{eff}	$t_{1/2}^{0\nu} (10^{29} \text{ y})$	
	pnQRPA	IBM-2
1.27	0.55–66.3	0.72–77.4
1.0	1.02–122	1.66–182

The ranges correspond to the adopted range of Majorana mass, $0.01 \text{ eV} < m_{\beta\beta} < 0.1 \text{ eV}$

final states, in this case the 0^+ ground states

$$M_K^{0\nu} = \left(0_{\text{gs},f}^+ \left\| \sum_{1,2} \mathcal{O}_K t_1^- t_2^- \right\| 0_{\text{gs},i}^+ \right) \tag{12}$$

with operators \mathcal{O}_K given in Eq. (10) and the closure energy enters the calculation through neutrino potential as discussed in Ref. [61]. Furthermore, in [61] the sensitivity of the $0\nu\beta\beta$ NME to the closure energy ($\sim 10 \text{ MeV}$) is estimated to be only 5 %, owing to the fact that the momentum of the virtual neutrino is of the order of 100–200 MeV, i.e., much larger than the typical nuclear excitations.

Since the effective value of the axial coupling g_A in finite nuclei is under debate [42,62,63], we calculate the $2\nu\beta\beta$ - and $0\nu\beta\beta$ -decay NMEs with two different effective g_A values: the free-nucleon value 1.27 and a standard "shell-model-type" quenched value 1.0. As can be seen from Eq. (5), the $2\nu\beta\beta$ -decay NME, once the Fermi part is forced to zero, does not directly depend on g_A . However, the g_A -dependence of the NME in the pnQRPA framework stems from the way we adjust the parameter g_{pp} , in the present case using the decay rate of a β -decay transition. On the other hand, $2\nu\beta\beta$ decay has now been measured in several nuclei, thus providing a way to estimate $g_{A,\text{eff},2\nu\beta\beta}^{\text{IBM-2}}$ by comparing experimental half-lives with theoretical IBM-2 predictions, as was done in Ref. [61]. The many-body states involved in the $0\nu\beta\beta$ -decay NMEs are corrected for the two-nucleon short-range correlations (SRCs) following the so-called CD-Bonn and Argonne parametrizations [64]. The resulting NMEs for $2\nu\beta\beta$ and $0\nu\beta\beta$ decays are shown in Tables 2 and 3, respectively. For $2\nu\beta\beta$ decay we also show the half-lives obtained from Eq. (4) with the calculated phase-space factors and NMEs. For comparison, we show the half-lives obtained in

Table 3 The $0\nu\beta\beta$ -decay NMEs for the transition $^{98}\text{Mo} \rightarrow ^{98}\text{Ru}$ calculated in the pnQRPA and IBM-2 frameworks with different short-range correlations (SRC) and values of g_A^{eff}

SRC	g_A^{eff}	pnQRPA					IBM-2				
		$M_F^{0\nu}$	$M_{\text{GT}}^{0\nu}$	$M_{\text{T}}^{0\nu}$	$M^{0\nu}$	$M^{0\nu}$	$M_F^{0\nu}$	$M_{\text{GT}}^{0\nu}$	$M_{\text{T}}^{0\nu}$	$M^{0\nu}$	$M^{0\nu}$
Argonne	1.27	-1.57	4.36	-0.38	4.95	4.95	-0.48	4.54	-0.26	4.58	4.58
Argonne	1.0	-1.58	4.72	-0.41	5.89	3.65	-0.48	4.62	-0.27	4.82	2.99
CD-Bonn	1.27	-1.69	4.76	-0.38	5.43	5.43	-0.52	4.70	-0.26	4.76	4.76
CD-Bonn	1.0	-1.69	5.17	-0.41	6.45	4.00	-0.52	4.78	-0.27	5.04	3.12

Here $M^{0\nu}$ refers to the so-called "effective" NME $(g_A^{\text{eff}}/g_A)^2 M^{0\nu}(g_A^{\text{eff}})$

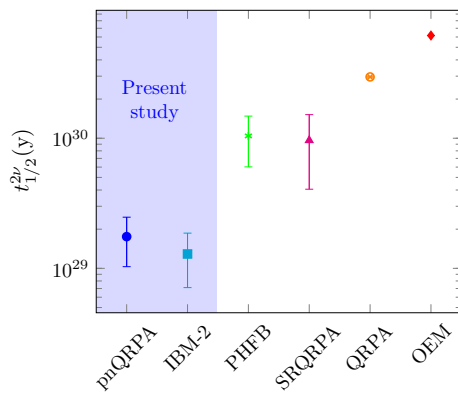


Fig. 4 The presently computed $2\nu\beta\beta$ -decay half-lives compared with earlier PHFB [65], SRQRPA [66], QRPA [67] and OEM [68] results. The ranges correspond to variation of $g_A = 1.0 - 1.27$

projected Hartree–Fock–Bogoliubov (PHFB) [65] and in the self-consistent renormalized QRPA (SRQRPA) [66] frameworks with less precise estimates for the phase-space factor. As for $0\nu\beta\beta$ -decay, it is hard to give estimates for the half-life, since it depends on the unknown Majorana mass (see Eq. (6)). Hence, in Table 4 we give estimates for the half-life for a Majorana mass range of $0.01 \text{ eV} < m_{\beta\beta} < 0.1 \text{ eV}$, which covers the part of the inverted-hierarchy band of Majorana mass allowed by cosmological searches – the region the next-generation experiments are interested in [19].

As can be seen from Table 2, the predicted half-lives of the $2\nu\beta\beta$ -decay are of the order of $t_{1/2}^{2\nu} \sim 10^{29}$ years – much longer than the currently observed half-lives in other nuclei, owing to the low Q -value $\sim 100 \text{ keV}$ of the presently discussed transition. For the measured decays the Q -values are of the order of $\sim 1 \text{ MeV}$. However, the differences between the pnQRPA and IBM-2 predictions are reasonable, IBM-2 giving some 15–20 % larger NMEs than pnQRPA. In Fig. 4, we compare the obtained half-lives with the available results obtained in other frameworks: the PHFB [65], SRQRPA [66], QRPA (with smaller single-particle bases) [67], and operator expansion model (OEM) [68]. The half-lives obtained in the present work are consistently smaller by a factor of ≈ 4 –35 than those obtained in the earlier works, mostly due to the larger NMEs obtained in the present work.

As for $0\nu\beta\beta$ decay, one can see from Table 3 that the pnQRPA-computed effective NMEs $M^{0\nu}$, obtained with $g_A^{\text{eff}} = 1.27$, are consistently larger by some 10–15% than the IBM-2-computed ones. With $g_A^{\text{eff}} = 1.0$ the difference is larger, 20–30%, owing to the g_{pp} -adjustment method of pnQRPA, which partially compensates the quenching effect. The differences between the two calculations stem from the quite different magnitudes of the Fermi NME, which is some 3 times larger in the pnQRPA formalism than in the IBM-2, owing to the quenching of the monopole term from the multiple expansion of the IBM-2 Fermi NME. The pnQRPA-

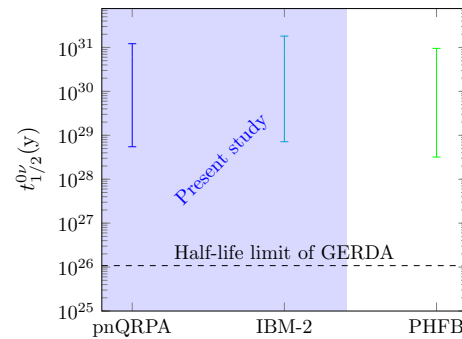


Fig. 5 The presently computed $0\nu\beta\beta$ -decay half-lives compared with earlier PHFB [69] results. The half-lives correspond to Majorana mass range $0.01 \text{ eV} < m_{\beta\beta} < 0.1 \text{ eV}$. For comparison, the half-life limit of GERDA experiment [11] – the current most stringent half-life limit for $0\nu\beta\beta$ decay – is shown

and IBM-2 -computed values of the Gamow-Teller NMEs are, however, quite close to each other. Interestingly, the NMEs obtained within both frameworks are smaller than the NMEs obtained in the PHFB framework [69], $M^{0\nu}(g_A^{\text{eff}} = 1.254) = 5.94 - 7.13$ and $M^{0\nu}(g_A^{\text{eff}} = 1.0) = 4.23 - 5.13$.

The $0\nu\beta\beta$ -decay half-life predictions in Table 4, obtained from Eq. (6) with the NMEs of Table 3 and the Majorana mass range $0.01 \text{ eV} < m_{\beta\beta} < 0.1 \text{ eV}$, are ranging between 0.55×10^{29} years and 1.82×10^{31} years. The smaller IBM-2 NMEs are reflected as slightly longer half-lives, but the ranges obtained in both frameworks are wide due to the uncertainty on the Majorana mass. The lower limits are similar to our half-life predictions for the $2\nu\beta\beta$ decay, but the upper limits are ~ 100 times larger. In any case, the half-lives are well beyond the half-life sensitivities of the current experiments $S_{1/2} \approx 10^{25} - 10^{26}$ years (for other nuclei). In Fig. 5, we compare the presently obtained half-life predictions with the prediction obtained with the PHFB-computed NMEs [69] and the above-mentioned Majorana mass range. In addition, we show the current most stringent $0\nu\beta\beta$ half-life limit, obtained for ^{76}Ge by the GERDA collaboration [11]. We notice that while the predictions obtained in the three different frameworks are in reasonable agreement, all of them are still far away from the current experiments’ reach.

4 Conclusion

We have determined the Q -value for the double-beta decay of ^{98}Mo directly for the first time using Penning-trap mass spectrometry. The obtained $Q_{\beta\beta} = 113.668(68) \text{ keV}$ agrees with the $Q_{\beta\beta}$ -value given in AME2020, $109(6) \text{ keV}$ [21], but is almost 90 times more precise. Based on the measured Q -value, the phase-space factors for the two-neutrino and neutrinoless double-beta-decay modes were computed. Furthermore, the nuclear matrix elements, involved in the half-

life expressions of these decay modes, were calculated in the pnQRPA and IBM-2 frameworks. Within both frameworks we take the isospin restoration into account by forcing the Fermi matrix element of the $2\nu\beta\beta$ decay to vanish.

The presently obtained $2\nu\beta\beta$ half-lives are consistently smaller than those previously obtained in the PHFB [69] or in the SQRPA [66] framework, mostly due to larger NMEs obtained in pnQRPA and IBM-2. On the other hand, the differences between the pnQRPA and IBM-2 values are relatively small, IBM-2 giving some 15–20% larger NMEs than pnQRPA. As for $0\nu\beta\beta$ decay, the NMEs obtained in pnQRPA and IBM-2 are consistently smaller than those obtained in the PHFB framework [69], but pnQRPA predicts some 10–30% larger NMEs, depending on the value of g_A^{eff} and the SRC-parametrization. This difference largely pertains to the marked differences in the Fermi NME, the Gamow–Teller NMEs being roughly equal. All in all, the predictions given by the two models are in satisfactory agreement, bearing in mind that the theoretical foundations of the two approaches are quite different: The IBM-2 using the closure approximation and a quite restricted single-particle space with renormalized transition operators, and the pnQRPA including explicitly the intermediate virtual states and using a large no-core single-particle space with bare transition operators. According to both models, the half-life of the $2\nu\beta\beta$ -decay of ^{98}Mo , corresponding to the presently obtained Q -value, would be notably larger than the currently known experimental half-lives of some other double-beta nuclei.

Acknowledgements This work has been supported by the Finnish Cultural Foundation (Grant No. 00210067) and the Academy of Finland (Grant Nos. 314733, 320062, 318043, 295207 and 327629). The funding from the European Union’s Horizon 2020 research and innovation programme under Grant agreement No. 771036 (ERC CoG MAIDEN) is gratefully acknowledged.

Funding Information Open Access funding provided by University of Jyväskylä (JYU).

Data Availability Statement This manuscript has no associated data or the data will not be deposited. [Author’s comment: The datasets generated during and/or analysed during the current study are available in the JYX repository, <https://doi.org/10.17011/jyx/dataset/80083>.]

Open Access This article is licensed under a Creative Commons Attribution 4.0 International License, which permits use, sharing, adaptation, distribution and reproduction in any medium or format, as long as you give appropriate credit to the original author(s) and the source, provide a link to the Creative Commons licence, and indicate if changes were made. The images or other third party material in this article are included in the article’s Creative Commons licence, unless indicated otherwise in a credit line to the material. If material is not included in the article’s Creative Commons licence and your intended use is not permitted by statutory regulation or exceeds the permitted use, you will need to obtain permission directly from the copyright holder. To view a copy of this licence, visit <http://creativecommons.org/licenses/by/4.0/>.

References

1. A. Barabash, Precise half-life values for two-neutrino double- β decay: 2020 review. *Universe* **6**, 159 (2020). <https://doi.org/10.3390/universe6100159>
2. E. Majorana, Sulla simmetria tra particelle e antiparticelle [in italian]. *Nuovo Cim.* **14**, 322 (1937)
3. M. Fukugita, T. Yanagida, Baryogenesis without grand unification. *Phys. Lett. B* **174**, 45 (1986). [https://doi.org/10.1016/0370-2693\(86\)91126-3](https://doi.org/10.1016/0370-2693(86)91126-3)
4. S. Davidson, E. Nardi, Y. Nir, Leptogenesis. *Phys. Rep.* **466**, 105 (2008). <https://doi.org/10.1016/j.physrep.2008.06.002>
5. F.T. Avignone III., S.R. Elliott, J. Engel, Double beta decay, Majorana neutrinos, and neutrino mass. *Rev. Mod. Phys.* **80**, 481 (2008). <https://doi.org/10.1103/RevModPhys.80.481>
6. J.D. Vergados, H. Ejiri, F. Šimkovic, Theory of neutrinoless double-beta decay. *Rep. Prog. Phys.* **75**, 106301 (2012). <https://doi.org/10.1088/0034-4885/75/10/106301>
7. J. Engel, J. Menéndez, Status and future of nuclear matrix elements for neutrinoless double-beta decay: a review. *Rep. Prog. Phys.* **80**, 046301 (2017). <https://doi.org/10.1088/1361-6633/aa5bc5>
8. M.J. Dolinski, A.W.P. Poon, W. Rodejohann, Neutrinoless double-beta decay: status and prospects. *Ann. Rev. Nucl. Part. Sci.* **69**, 219 (2019). <https://doi.org/10.1146/annurev-nucl-101918-023407>
9. H. Ejiri, J. Suhonen, K. Zuber, Neutrino–nuclear responses for astro-neutrinos, single beta decays and double beta decays. *Phys. Rep.* **797**, 1 (2019). <https://doi.org/10.1016/j.physrep.2018.12.001>
10. D. Q. Adams, et al., (CUORE Collaboration), High sensitivity neutrinoless double-beta decay search with one tonne-year of CUORE data (2021). [arXiv:2104.06906](https://arxiv.org/abs/2104.06906)
11. M. Agostini et al., (GERDA Collaboration), Final results of GERDA on the search for neutrinoless double- β decay. *Phys. Rev. Lett.* **125**, 252502 (2020). <https://doi.org/10.1103/PhysRevLett.125.252502>
12. G. Anton et al., (EXO-200 Collaboration), Search for neutrinoless double- β decay with the complete EXO-200 dataset. *Phys. Rev. Lett.* **123**, 161802 (2019). <https://doi.org/10.1103/PhysRevLett.123.161802>
13. S.I. Alvis et al., (MAJORANA Collaboration), Search for neutrinoless double- β decay in ^{76}Ge with 26 kg yr of exposure from the MAJORANA DEMONSTRATOR. *Phys. Rev. C* **100**, 025501 (2019). <https://doi.org/10.1103/PhysRevC.100.025501>
14. O. Azzolini et al., (CUPID Collaboration), Final result of CUPID-0 Phase-I in the search for the ^{82}Se neutrinoless double- β decay. *Phys. Rev. Lett.* **123**, 032501 (2019). <https://doi.org/10.1103/PhysRevLett.123.032501>
15. R. Arnold et al., (NEMO Collaboration), Measurement of the $2\nu\beta\beta$ decay half-life and search for the $0\nu\beta\beta$ decay of ^{116}Cd with the NEMO-3 detector. *Phys. Rev. D* **95**, 012007 (2017)
16. A. Gando et al., (KamLAND-Zen Collaboration), Search for Majorana neutrinos near the inverted mass hierarchy region with KamLAND-Zen. *Phys. Rev. Lett.* **117**, 082503 (2016). <https://doi.org/10.1103/PhysRevLett.117.082503>
17. M. Agostini, A.M. Bakalyarov, M. Balata, I. Barabanov, L. Baudis et al., Probing Majorana neutrinos with double- β decay. *Science* **365**, 1445–1448 (2019). <https://doi.org/10.1126/science.aav8613>
18. S.D. Biller, Combined constraints on Majorana masses from neutrinoless double beta decay experiments. *Phys. Rev. D* **104**, 012002 (2021). <https://doi.org/10.1103/PhysRevD.104.012002>
19. M. Agostini, G. Benato, J.A. Detwiler, J. Menéndez, F. Vissani, Testing the inverted neutrino mass ordering with neutrinoless double-beta decay. *Phys. Rev. C* **104**, L042501 (2021). <https://doi.org/10.1103/PhysRevC.104.L042501>

20. J. Kotila, F. Iachello, Phase-space factors for double- β decay. *Phys. Rev. C* **85**, 034316 (2012). <https://doi.org/10.1103/PhysRevC.85.034316>
21. M. Wang, W. Huang, F. Kondev, G. Audi, S. Naimi, The AME 2020 atomic mass evaluation (II). Tables, graphs and references. *Chin. Phys. C* **45**(3), 030003 (2021). <https://doi.org/10.1088/1674-1137/abddaf>
22. R.A. Damerow, R.R. Ries, W.H. Johnson, Atomic masses from ruthenium to xenon. *Phys. Rev.* **132**, 1673–1681 (1963). <https://doi.org/10.1103/PhysRev.132.1673>
23. T. Eronen et al., JYFLTRAP: a Penning trap for precision mass spectroscopy and isobaric purification. *Eur. Phys. J. A* **48**(4), 46 (2012). <https://doi.org/10.1140/epja/i2012-12046-1>
24. S. Eliseev, D. Nesterenko, K. Blaum, M. Block, C. Droese, F. Herfurth, E. Minayaramirez, Y.N. Novikov, L. Schweikhard, K. Zuber, Q values for neutrinoless double-electron capture in ^{96}Ru , ^{162}Er , and ^{168}Yb . *Phys. Rev. C* **83**, 038501 (2011). <https://doi.org/10.1103/PhysRevC.83.038501>
25. J. Hyvärinen, J. Suhonen, Nuclear matrix elements for $0\nu\beta\beta$ decays with light or heavy Majorana-neutrino exchange. *Phys. Rev. C* **91**, 024613 (2015). <https://doi.org/10.1103/PhysRevC.91.024613>
26. F. Šimkovic, A. Faessler, V. Rodin, P. Vogel, J. Engel, Anatomy of the $0\nu\beta\beta$ nuclear matrix elements. *Phys. Rev. C* **77**, 045503 (2008). <https://doi.org/10.1103/PhysRevC.77.045503>
27. J. Barea, F. Iachello, Neutrinoless double-beta decay in the microscopic interacting boson model. *Phys. Rev. C* **79**, 044301 (2009). <https://doi.org/10.1103/PhysRevC.79.044301>
28. J. Barea, J. Kotila, F. Iachello, $0\nu\beta\beta$ and $2\nu\beta\beta$ nuclear matrix elements in the interacting boson model with isospin restoration. *Phys. Rev. C* **91**(3), 034304 (2015). <https://doi.org/10.1103/PhysRevC.91.034304> arXiv:1506.08530
29. I. Moore et al., Towards commissioning the new IGISOL-4 facility. *Nucl. Instrum. Methods Phys. Res. B* **317**, 208–213 (2013). <https://doi.org/10.1016/j.nimb.2013.06.036>
30. S. Rahaman, V.-V. Elomaa, T. Eronen, J. Hakala, A. Jokinen, J. Julin, A. Kankainen, A. Saastamoinen, J. Suhonen, C. Weber, J. Äystö, Q values of the ^{76}Ge and ^{100}Mo double-beta decays. *Phys. Lett. B* **662**(2), 111–116 (2008). <https://doi.org/10.1016/j.physletb.2008.02.047>
31. M. Vilén et al., A new off-line ion source facility at IGISOL. *Nucl. Instrum. Methods Phys. Res. Sect. B* (2020). <https://doi.org/10.1016/j.nimb.2019.04.051>
32. A. Nieminen, J. Huikari, A. Jokinen, J. Äystö, P. Campbell, E. Cochrane, Beam cooler for low-energy radioactive ions. *Nucl. Instrum. Methods Phys. Res. A* **469**(2), 244–253 (2001). [https://doi.org/10.1016/S0168-9002\(00\)00750-6](https://doi.org/10.1016/S0168-9002(00)00750-6)
33. G. Savard, S. Becker, G. Bollen, H.J. Kluge, R.B. Moore, T. Otto, L. Schweikhard, H. Stolzenberg, U. Wiess, A new cooling technique for heavy ions in a Penning trap. *Phys. Lett. A* **158**(5), 247–252 (1991). [https://doi.org/10.1016/0375-9601\(91\)91008-2](https://doi.org/10.1016/0375-9601(91)91008-2)
34. S. Eliseev, K. Blaum, M. Block, C. Droese, M. Goncharov, E. Minaya Ramirez, D.A. Nesterenko, Y.N. Novikov, L. Schweikhard, Phase-imaging ion-cyclotron-resonance measurements for short-lived nuclides. *Phys. Rev. Lett.* **110**, 082501 (2013). <https://doi.org/10.1103/PhysRevLett.110.082501>
35. S. Eliseev et al., A phase-imaging technique for cyclotron-frequency measurements. *Appl. Phys. B* **114**(1), 107–128 (2014). <https://doi.org/10.1007/s00340-013-5621-0>
36. D.A. Nesterenko et al., Phase-Imaging Ion-Cyclotron-Resonance technique at the JYFLTRAP double Penning trap mass spectrometer. *Eur. Phys. J. A* **54**, 154 (2018). <https://doi.org/10.1140/epja/i2018-12589-y>
37. D. Nesterenko, T. Eronen, Z. Ge, A. Kankainen, M. Vilén, Study of radial motion phase advance during motion excitations in a penning trap and accuracy of JYFLTRAP mass spectrometer. *Eur. Phys. J. A* **57**, 302 (2021). <https://doi.org/10.1140/epja/s10050-021-00608-3>
38. C. Roux et al., Data analysis of Q -value measurements for double-electron capture with SHIPTRAP. *Eur. Phys. J. D* **67**(7), 146 (2013). <https://doi.org/10.1140/epjd/e2013-40110-x>
39. A. Kellerbauer, K. Blaum, G. Bollen, F.H.H.-J. Kluge, M. Kuckein, E. Sauvan, C. Scheidenberger, L. Schweikhard, From direct to absolute mass measurements: a study of the accuracy of ISOLTRAP. *Eur. Phys. J. D* **22**, 53–64 (2003). <https://doi.org/10.1140/epjd/e2002-00222-0>
40. NIST, Atomic spectra database <https://doi.org/10.18434/T4W30F>, <https://www.nist.gov/pml/atomic-spectra-database>. Accessed 8 Mar 2022
41. W. Huang, M. Wang, F. Kondev, G. Audi, S. Naimi, The AME 2020 atomic mass evaluation (i). Evaluation of input data, and adjustment procedures. *Chin. Phys. C* **45**(3), 030002 (2021). <https://doi.org/10.1088/1674-1137/abddb0>
42. J.T. Suhonen, Value of the axial-vector coupling strength in β and β decays: a review. *Front. Phys.* **5**, 55 (2017)
43. M. Doi, T. Kotani, H. Nishiura, K. Okuda, E. Takasugi, Neutrino Mass, the Right-Handed Interaction and the Double Beta Decay. I: Formalism. *Progr. Theor. Phys.* **66** (5) (1981) 1739–1764. <https://doi.org/10.1143/PTP.66.1739>
44. M. Doi, T. Kotani, H. Nishiura, E. Takasugi, Double Beta Decay. *Progr. Theor. Phys.* **69** (2) (1983) 602–635. <https://doi.org/10.1143/PTP.69.602>
45. H. Primakoff, S.P. Rosen, Double beta decay. *Rep. Progr. Phys.* **22**(1), 121–166 (1959). <https://doi.org/10.1088/0034-4885/22/1/305>
46. T. Tomoda, Double beta decay. *Rep. Progress Phys.* **54**(1), 53–126 (1991). <https://doi.org/10.1088/0034-4885/54/1/002>
47. F. Boehm, P. Vogel, *Physics of Massive Neutrinos*, 2nd edn. (Cambridge University Press, Cambridge, 1992). <https://doi.org/10.1017/CBO9780511622571>
48. M. Doi, T. Kotani, E. Takasugi, Double Beta Decay and Majorana Neutrino. *Progr. Theor. Phys. Suppl.* **83** (1985) 1–175. <https://doi.org/10.1143/PTPS.83.1>
49. L. Jokiniemi, H. Ejiri, D. Frekers, J. Suhonen, Neutrinoless $\beta\beta$ nuclear matrix elements using isovector spin-dipole $J^\pi = 2^-$ data. *Phys. Rev. C* **98**, 024608 (2018). <https://doi.org/10.1103/PhysRevC.98.024608>
50. L. Jokiniemi, J. Suhonen, Muon-capture strength functions in intermediate nuclei of $0\nu\beta\beta$ decays. *Phys. Rev. C* **100**, 014619 (2019). <https://doi.org/10.1103/PhysRevC.100.014619>
51. A. Bohr, B.R. Mottelson, *Nuclear Structure*, vol. I (Benjamin, New York, 1969)
52. K. Holinde, Two-nucleon forces and nuclear matter. *Phys. Rep.* **68**, 121 (1981). [https://doi.org/10.1016/0370-1573\(81\)90188-5](https://doi.org/10.1016/0370-1573(81)90188-5)
53. J. Suhonen, O. Civitarese, Weak interaction and nuclear structure aspects of nuclear double beta decay. *Phys. Rep.* **300**, 123 (1998)
54. F. Šimkovic, V. Rodin, A. Faessler, P. Vogel, $0\nu\beta\beta$ and $2\nu\beta\beta$ nuclear matrix elements, quasiparticle random-phase approximation, and isospin symmetry restoration. *Phys. Rev. C* **87**, 045501 (2013). <https://doi.org/10.1103/PhysRevC.87.045501>
55. J. Suhonen, *From Nucleons to Nucleus: Concepts of Microscopic Nuclear Theory* (Springer, Berlin, 2007)
56. A. Arima, T. Ohtsuka, F. Iachello, I. Talmi, Collective nuclear states as symmetric couplings of proton and neutron excitations. *Phys. Lett. B* **66**(3), 205–208 (1977). [https://doi.org/10.1016/0370-2693\(77\)90860-7](https://doi.org/10.1016/0370-2693(77)90860-7)
57. F. Iachello, A. Arima, *The Interacting Boson Model* (Cambridge University Press, Cambridge, 1987)
58. T. Otsuka, A. Arima, F. Iachello, Nuclear shell model and interacting bosons. *Nucl. Phys. A* **309**(1), 1–33 (1978). [https://doi.org/10.1016/0375-9474\(78\)90532-8](https://doi.org/10.1016/0375-9474(78)90532-8)
59. J. Kotila, J. Barea, Occupation probabilities of single particle levels using the microscopic interacting boson model: application to some

- nuclei of interest in neutrinoless double- β decay. *Phys. Rev. C* **94**, 034320 (2016). <https://doi.org/10.1103/PhysRevC.94.034320>
60. J. Engel, Uncertainties in nuclear matrix elements for neutrinoless double-beta decay. *J. Phys. G Nucl. Part. Phys.* **42**(3), 034017 (2015). <https://doi.org/10.1088/0954-3899/42/3/034017>
61. J. Barea, J. Kotila, F. Iachello, Nuclear matrix elements for double- β decay. *Phys. Rev. C* **87**(1), 014315 (2013). <https://doi.org/10.1103/PhysRevC.87.014315> arXiv:1301.4203
62. I.S. Towner, *Phys. Rep.* **155**, 263–377 (1987). [https://doi.org/10.1016/0370-1573\(87\)90138-4](https://doi.org/10.1016/0370-1573(87)90138-4)
63. J. Suhonen, J. Kostensalo, Double β decay and the axial strength. *Front. Phys.* **7**, 29 (2019)
64. F. Šimkovic, A. Faessler, H. Müther, V. Rodin, M. Stauf, $0\nu\beta\beta$ -decay nuclear matrix elements with self-consistent short-range correlations. *Phys. Rev. C* **79**, 055501 (2009). <https://doi.org/10.1103/PhysRevC.79.055501>
65. R. Chandra, J. Singh, P. Rath, P. Raina, J. Hirsch, Two-neutrino double- β decay of $94 \leq A \leq 110$ nuclei for the $0^+ \rightarrow 0^+$ transition. *Eur. Phys. J. A* **23**, 223 (2005). <https://doi.org/10.1140/epja/i2004-10087-7>
66. A. Bobyk, W. Kamiński, P. Zaręba, Study of the double beta decay of $70 \leq A \leq 100$ nuclei within the QRPA and the self-consistent BCS + QRPA formalisms. *Nucl. Phys. A* **669**, 221 (2000). [https://doi.org/10.1016/S0375-9474\(99\)00820-9](https://doi.org/10.1016/S0375-9474(99)00820-9)
67. A. Staudt, K. Muto, H.V. Klapdor, Calculation of 2ν and 0ν Double-Beta Decay Rates. *Europhys. Lett.* **13**, 31 (1990). <https://doi.org/10.1209/0295-5075/13/1/006>
68. M. Hirsch, R. Wua, H.V. Klapdor-Kleingrothaus, C. Cheng-rui, Operator expansion method and nuclear $\beta\beta$ decay. *Phys. Rep.* **242**, 403 (1994). [https://doi.org/10.1016/0370-1573\(94\)90174-0](https://doi.org/10.1016/0370-1573(94)90174-0)
69. P.K. Rath, R. Chandra, K. Chaturvedi, P. Lohani, P.K. Raina, J.G. Hirsch, Neutrinoless $\beta\beta$ decay transition matrix elements within mechanisms involving light majorana neutrinos, classical majorons, and sterile neutrinos. *Phys. Rev. C* **88**, 064322 (2013). <https://doi.org/10.1103/PhysRevC.88.064322>